PASJ: Publ. Astron. Soc. Japan **52**, 329–336 (2000)

Two-Epoch Space VLBI Observations of the Gamma-Ray Loud Quasar PKS 1741−038

Kiyoaki WAJIMA,[1,2] James E.J. LOVELL,[3] Hideyuki KOBAYASHI,[4]
Hisashi HIRABAYASHI,[2] Kenta FUJISAWA,[4] and Masato TSUBOI[1]

[1] *Institute of Astrophysics and Planetary Science, Ibaraki University, Bunkyo, Mito, Ibaraki 310-8512*
[2] *The Institute of Space and Astronautical Science, 3-1-1 Yoshinodai, Sagamihara, Kanagawa 229-8510*
[3] *Australia Telescope National Facility, CSIRO, PO Box 76, Epping NSW 1710, Australia*
[4] *National Astronomical Observatory, 2-21-1 Osawa, Mitaka, Tokyo 181-8588*
E-mail (KW): kiyoaki@vsop.isas.ac.jp

(Received 1999 November 18; accepted 1999 December 24)

Abstract

We present the results of high-resolution imaging of the gamma-ray loud quasar PKS 1741−038 with the HALCA satellite and ground radio telescopes. Observations were made at two epochs at an interval of nine months with the first-epoch observation at 1.6 and 5 GHz and with the second-epoch observation at 5 GHz. The source shows a very compact structure, but is clearly resolved in the space–ground baseline visibility data. The core component of the source has a brightness temperature, $T_{\rm b}$, greater than 10^{12} K in the source's rest frame at each frequency. We applied three individual jet models in order to derive the Doppler factor, δ. The core component has $\delta \sim 14$, considering the $T_{\rm b}$ limit due to the inverse Compton catastrophe, while a 2.5-times larger δ is obtained assuming that the particles and magnetic field are in equipartition. Two-epoch images at 5 GHz show almost no change of the structure. Assuming that the component motion in this interval is less than our resolution, we derived the upper limit of the viewing angle as being 4.°8. The smaller viewing angle and higher Doppler factor favor the inverse Compton gamma-ray emission model; we conclude that the gamma-ray emission from this source is highly Doppler-boosted.

Key words: galaxies: active — galaxies: nuclei — quasars: individual (PKS 1741−038)

1. Introduction

Observations made with the Energetic Gamma Ray Experiment Telescope (EGRET) onboard the Compton Gamma Ray Observatory (CGRO) have revealed the existence of 67 gamma-ray loud AGNs (Hartman et al. 1999). These are predominantly radio-loud AGNs, implying that there is a strong connection between the gamma-ray emission and the radio emission. All AGNs, however, such as BL Lacertae objects or optical violent variables, which have strong activity at radio wavelengths, do not always have gamma-ray emission (e.g. von Montigny et al. 1995). The difference between gamma-ray loud and quiet AGNs is not definite, and it is important to clarify this point in order to understand the physical properties of AGN, such as the energy production and radiation mechanism.

There are two likely mechanisms of gamma-ray emission from AGNs. One is the synchrotron self-Compton model (Königl 1981), in which seed photons are provided from synchrotron radiation, which are boosted to gamma-ray energies by inverse Compton scattering due to synchrotron-emitting particles. The other is Comptonization of external radiation from an accretion disk or broad-line region clouds around a central engine (Sikora et al. 1994). In either case, they need smaller viewing angles and higher Doppler factors in order that the observer may stand within the gamma-ray emission beam. Recent statistical research implies that limited samples of gamma-ray loud AGNs have smaller viewing angles and higher Doppler factors than gamma-ray quiet AGNs (Jiang et al. 1998). However, their sample has only 18 gamma-ray loud AGNs, for which the angular size, radio flux density of the VLBI core, and proper motion of the components in the jet had been measured. It is therefore important to verify the VLBI-scale properties for individual sources precisely.

PKS 1741−038 (OT–68) is one of the EGRET sources with a high-confidence identification (Hartman et al. 1999). It is a strong, compact radio source identified as a core-dominated highly polarized quasar (Impey, Tapia 1990) with redshift $z = 1.054$ (White et al. 1988).

In this paper, we report on the results of two-epoch VSOP (VLBI Space Observatory Programme;

Table 1. Observation summary.

Date	Telescopes	Frequency (GHz)	Correlator	Total observing time
1997 July 5 (epoch 1)	HALCA, VLBA	1.6, 5	VLBA, Socorro	4^h44^m (5 GHz) 4^h11^m (1.6 GHz)
1998 April 6 (epoch 2)	HALCA, Hobart, Shanghai, Mopra	5	S2, Penticton	5^h54^m

Hirabayashi et al. 1998) observations of PKS 1741−038. VSOP consists of the radio-astronomy satellite HALCA and ground radio telescopes located around the world. HALCA has an elliptical orbit with an apogee height of 21400 km, a perigee height of 560 km, and an orbital period of 6.3 hr. This enables a close look at the compact core of AGNs, with a factor of ~ 3 improvement in the resolution compared to ground-only VLBI observations at the same frequencies. PKS 1741−038 is near to the celestial equator, and ground-based VLBI observations tend to have poorer u–v coverage in the north–south baselines; however, VSOP observation can obtain a much better angular resolution for the north–south direction by choosing a good observing epoch.

Throughout this paper, we define the spectral index, α, as $S_\nu \propto \nu^\alpha$, and we assume the Hubble constant, H_0, to be 100 h km s^{-1} Mpc^{-1} and the deceleration parameter, q_0, to be 0.5, which implies an angular-to-linear scale conversion of 4.24 h^{-1} pc mas^{-1} for PKS 1741−038.

2. Observations and Data Reduction

2.1. *VSOP Observations*

PKS 1741−038 was observed with VSOP in left-circular polarization at 1.6 and 5 GHz on 1997 July 5 (hereafter epoch 1), and at 5 GHz on 1998 April 6 (hereafter epoch 2). An observation summary is given in table 1. The ground radio telescopes (GRTs) of epoch 1 were the VLBA (Very Long Baseline Array), and HALCA tracking stations in Green Bank (USA), Goldstone (USA), and Usuda (Japan) were used; the data were recorded in the VLBA format. The data at epoch 1 were correlated at the VLBA correlator in Socorro with an output preaveraging time of 0.524 and 1.966 s for the space–ground and ground–ground baselines, respectively. The GRTs of epoch 2 were Hobart (Australia), Mopra (Australia), and Shanghai (China) and the tracking stations in Goldstone and Tidbinbilla (Australia) were used; the data were recorded in the S2 format. The data at epoch 2 were correlated at the S2 correlator in Penticton with an output preaveraging time of 0.1 and 2 s for the space–ground and ground–ground baselines, respectively. Observations were made with a total observing bandwidth of 32 MHz divided into two intermediate frequency (IF) bands. In epoch 1, one of the HALCA's IFs was used for 1.6 GHz and the other for 5 GHz. At VLBA, the observing frequency was switched every one hour between 1.6 and 5 GHz with an effective observation time at each frequency of about 4.5 hr.

Table 2. Fringe detection limits.

Epoch	Frequency (GHz)	Baseline	7σ limit (mJy)
1	1.6	ground only	39
		space–ground	410
	5	ground only	21
		space–ground	220
2	5	ground only	36
		space–ground	190

2.2. *Fringe Fitting*

Post-processing of the correlated data was done in NRAO AIPS and DIFMAP (Shepherd et al. 1994). We applied an amplitude calibration using the antenna gain factors and system temperature measurements. Although one IF band has 256 spectral channels, we did not use the data from 1 to 40 and 210 to 256 channels in each IF. This reduced the total observing bandwidth to 21.1 MHz. In a fringe-fitting run, a solution interval of three minutes and a point-source model were employed. The VLBA antenna at Pie Town (PT) and Hobart served as reference telescopes at epochs 1 and 2, respectively. The 7σ fringe-detection limits for each observation are listed in table 2. The fringe-detection limit for the ground–ground baseline at epoch 1 is better than that of epoch 2, while it is vice versa for the space–ground baseline. This is because the observing frequency was switched at the VLBA in epoch 1, as shown in subsection 2.1; this halves the total observing band of the space–ground observation. Fringes were detected in all ground–ground baselines and in space–ground baselines, except for the Usuda tracking station data. We therefore excluded the Usuda tracking data when imaging.

Table 3. Map descriptions.

Epoch (1)	Frequency (GHz) (2)	S_{peak} (Jy beam^{-1}) (3)	Major (mas) (4)	Minor (mas) (5)	P.A. (deg) (6)	Contours (mJy beam^{-1}) (7)
1	1.6	1.31	2.66	0.86	25	11×2^n ($n = 0, 1, ..., 6$)
	5	2.93	0.92	0.41	32	17×2^n ($n = 0, 1, ..., 7$)
2	5	1.82	0.73	0.23	8	$-12, 12 \times 2^n$ ($n = 0, 1, ..., 6$)

Note.
(1) Observation epoch.
(2) Observation frequency.
(3) Peak flux density.
(4)–(6) Major and minor axes and the position angle of the restoring beam.
(7) Contour levels of the map.

2.3. *Imaging*

Fringe-fitted visibility data were exported from AIPS to DIFMAP for imaging. The data were integrated over 30 s to reconcile the different preaveraging time from the correlator output. Several iterations of cleaning and self-calibration to phases (and amplitudes in the later stages) were performed. To ensure a better angular resolution with the HALCA data, uniform weighting of the data was adopted with gridding weights scaled by amplitude errors raised to the power of −1. Figure 1 displays the u–v coverages for the 5 GHz experiments at each epoch. The inner tracks correspond to the baselines between the ground radio telescopes, while the outer tracks indicate the space–ground baselines which enable a higher angular resolution along with a dramatic improvement of the u–v coverage. Our VSOP images obtain dynamic ranges (ratio of the highest to the lowest brightness levels in the image) of 360, 430, and 150 for the 1.6 and 5 GHz observations of epoch 1 and 5 GHz of epoch 2, respectively. Each image is shown in figure 2 and the detailed parameters of the images are summarized in table 3.

3. Results

Figures 2a and b show the 1.6 GHz VSOP image of PKS 1741−038 and the visibility amplitude as a function of the u–v distance. Our image has one compact, bright component. However, from figure 2b we can see that the visibility amplitude at the maximum space–ground baseline is ∼ 35% of the zero-baseline flux density, and that the source is clearly resolved.

Figures 2c and d show the 5 GHz VSOP image of PKS 1741−038 and the visibility amplitude as a function of the u–v distance at epoch 1. Our image also has one compact, bright component. From figure 2d we can see that the visibility amplitude at the maximum space–ground baseline is ∼ 20% of the zero-baseline flux density, and that the source is clearly resolved. We can also see in figure 2d that the visibility amplitude at ∼ 140 Mλ is different between that at the ground–ground baselines and that at the space–ground baselines. The former corresponds to the east–west direction in the u–v plane, and the latter to the north–south direction (see figure 1). This implies that the source has an elongated structure in the north–south direction. The zero-baseline flux density in our observation is 4.2 Jy. Single-dish measurements from the University of Michigan Radio Astronomy Observatory (UMRAO) show 4.8 GHz flux densities of PKS 1741−038 as 3.60 ± 0.11 Jy on 1997 May 29, and 3.87 ± 0.04 Jy on 1997 August 5. The calibration uncertainties are likely to be a cause of some of this discrepancy; however, we note that 4.8 GHz flux densities from UMRAO on 1997 April 30, May 10, and May 16 are 3.90 ± 0.08 Jy, 4.35 ± 0.12 Jy, and 3.69 ± 0.07 Jy, respectively, indicating a significant short-term variability in this source. The spectral index between the zero-baseline flux densities of 1.6 and 5 GHz in our observation is +0.5.

Figures 2e and f show the 5 GHz VSOP image of PKS 1741−038 and the visibility amplitude as a function of the u–v distance at epoch 2. Our image also shows a point-like structure, but the visibility amplitude drops to ∼ 1 Jy at the maximum space–ground baseline. The 4.8 GHz flux density from UMRAO on 1998 March 29 is 4.48 ± 0.04 Jy and our observation has a zero-baseline flux density of ∼ 3.7 Jy. Although there may be some amplitude calibration error, because only two of the four antennas measured the system noise temperature simultaneously, our result shows that the source is highly core-dominated.

This source has been imaged by some ground VLBI observations (e.g. Fey et al. 1996 at 2 and 8 GHz; Shen et al. 1997 at 5 GHz). Their VLBI images show one compact, bright component with a very diffused jet-like structure. On the other hand, a larger scale structure, such as kpc-scale radio lobes, has not been reported.

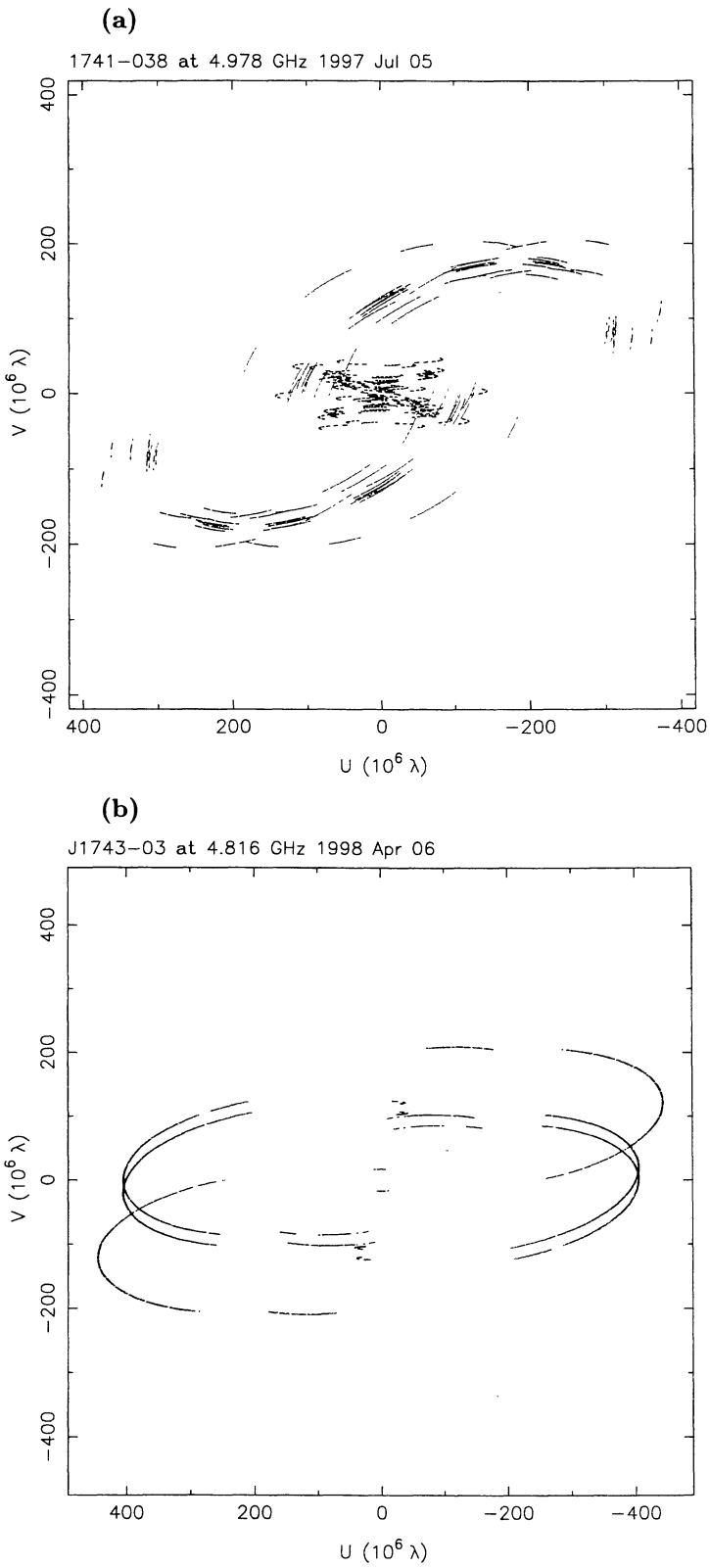

Fig. 1. u–v coverage for epoch 1 (a) and epoch 2 (b) observations at 5 GHz of PKS 1741−038.

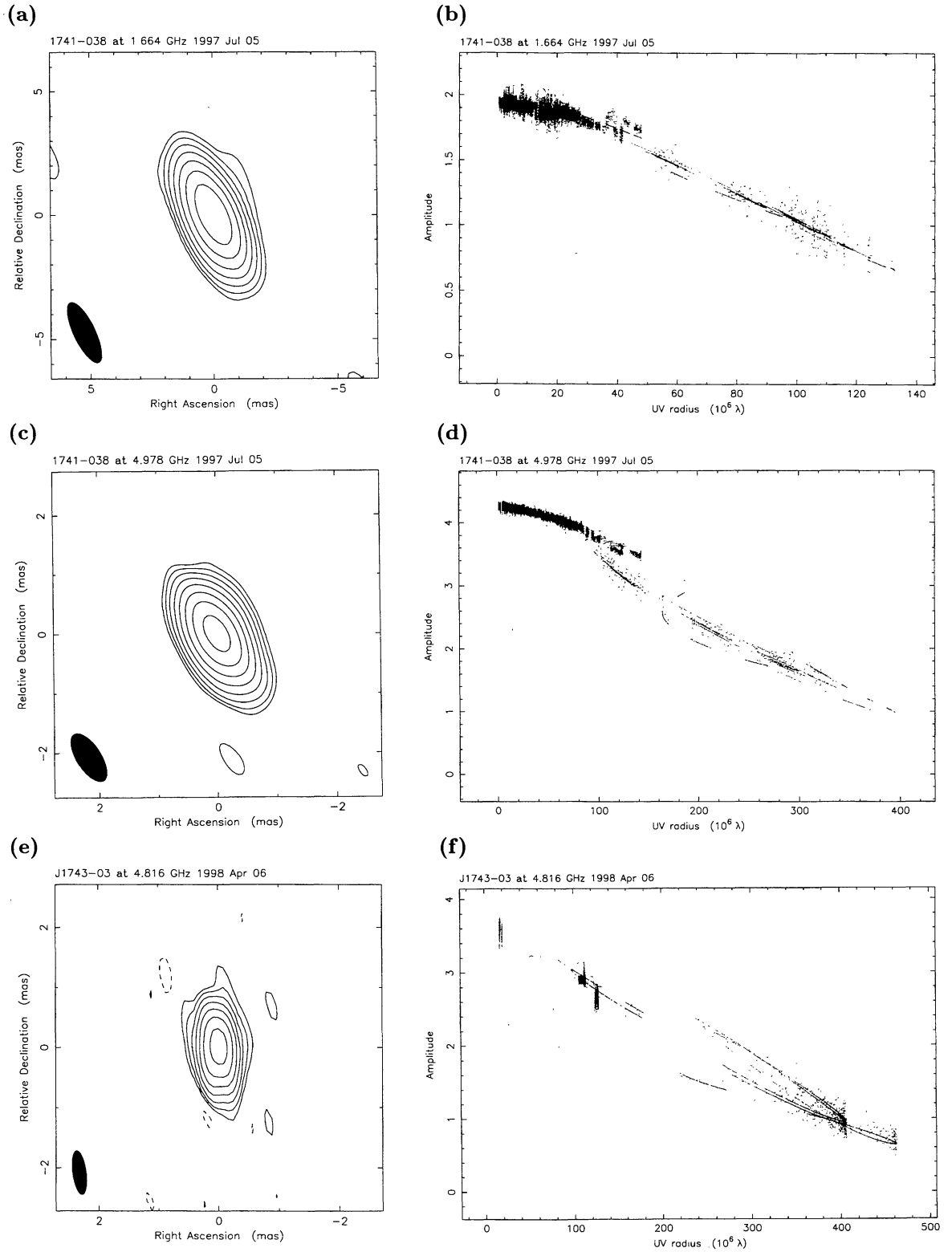

Fig. 2. VSOP images of PKS 1741−038 (left) and correlated flux density (Jy) versus projected baseline length (right). The plot shows the model fitting (solid curves) to the visibility amplitude as a function of the u–v distance. (a), (b) 1.6 GHz observation at epoch 1997.51 (1997 July 5) with the VLBA. (c), (d) 5 GHz observation at epoch 1997.51 (1997 July 5) with the VLBA. (e), (f) 5 GHz observation at epoch 1998.26 (1998 April 6) with Hobart, Shanghai, and Mopra. The detailed parameters are summarized in table 3.

Table 4. Model fitting results.

Epoch (1)	Frequency (GHz) (2)	Component (3)	S (Jy) (4)	r (mas) (5)	ϕ (deg) (6)	$\theta_{\rm maj}$ (mas) (7)	Ratio (8)	P.A. (deg) (9)	$T_{\rm b}$ (10^{11} K) (10)
1	1.6	1	1.93 ± 0.21	0	0	1.06 ± 0.15	0.80 ± 0.06	16 ± 4	20 ± 4
	5	1	4.23 ± 0.13	0	0	0.48 ± 0.08	0.69 ± 0.05	15 ± 5	28 ± 8
2	5	1	3.04 ± 0.54	0	0	0.35 ± 0.08	0.75 ± 0.05	-24 ± 6	34 ± 8
		2	0.59 ± 0.21	0.40 ± 0.20	163 ± 2	0.80 ± 0.37	1.0	–	0.9 ± 0.3

(1) Observation epoch.
(2) Observation frequency.
(3) Component number; component 1 is taken to be the core.
(4) Flux density of each component.
(5) Distance of each component from the origin defined by component 1
(6) Position angle of each component with respect to the origin (east of north).
(7)–(9) Parameters of Gaussian model: major axis in mas (FWHM), ratio of minor to major axes, and the position angle (P.A.) of the major axis.
(10) Peak brightness temperature given in the rest frame of the host galaxy.

Although our VSOP images, which have a highly core-dominated structure, are consistent with these previous results, the source is clearly resolved at visibility data from the space–ground baseline at each frequency (see figures 2b, d, and f).

4. Discussion

4.1. Brightness Temperature Estimation and Comparison with Other Observations

In order to derive the source size and the brightness temperature we applied a model consisting of some elliptical Gaussian components to the calibrated visibility data for each experiment. Table 4 gives the model fitting results. From these parameters we can calculate the source brightness temperature in the source's rest frame, $T_{\rm b}$, as follows:

$$T_{\rm b} = 1.41 \times 10^9 (1+z)(\theta_{\rm maj}\theta_{\rm min})^{-1} S\lambda^2 \quad {\rm K}, \qquad (1)$$

where $\theta_{\rm maj}$ and $\theta_{\rm min}$ are the FWHM sizes of the component in the major and minor axes in milliarcseconds, S is the flux density of the Gaussian component in Jy, and λ is the observed wavelength in centimeters. The brightness temperature results are also shown in table 4. We obtain $T_{\rm b} = (20 \pm 4)$, (28 ± 8), $(34 \pm 8) \times 10^{11}$ K for 1.6 GHz, 5 GHz epoch 1, and 5 GHz epoch 2, respectively.

PKS 1741−038 has been imaged with the SHEVE (Southern Hemisphere VLBI Experiments) network at 5 GHz (Shen et al. 1997), and the core component has had a brightness temperature of 11×10^{11} K. This source has also been observed by the 10000 km baseline global VLBI as a part of the VSOP pre-launch survey at 22 GHz (Moellenbrock et al. 1996) and the 18000 km baseline TDRSS-OVLBI (Tracking and Data Relay Satellite System–Orbiting VLBI) experiments at 2.3 GHz (Linfield et al. 1989); each observation shows a high brightness temperature in the core component of this source, $9.2^{+4.1}_{-2.1} \times 10^{11}$ K and $5.6^{+1.3}_{-1.0} \times 10^{11}$ K in the source's rest frame, respectively. The above mentioned experiments were very much limited to a u–v coverage, and the obtained results are based on a crude model fitting. Our $T_{\rm b}$ results are slightly higher than these, but we believe that our value is much more reliable. The long-term flux density profile of UMRAO shows that PKS 1741−038 has the minimum flux density near to the middle of 1992, and that the maximum flux density is near to the middle of 1998 at 4.8 GHz. The minimum flux density is caused by an extreme scattering event (ESE), as reported by Clegg et al. (1996). Shen et al. (1997), and Moellenbrock et al. (1996) observed this source on 1992 November and 1993 August, respectively. The UMRAO flux densities near to our 5 GHz VSOP observations are about 1.7-times greater than those of the UMRAO observations near to their epochs. The higher brightness temperature in our observation is likely to be an intrinsic effect.

4.2. Doppler Factor

As derived above, PKS 1741−038 has a high brightness temperature of $T_{\rm b} \sim 3 \times 10^{12}$ K at 5 GHz VSOP observations. Ground-based VLBI measurements of the brightness temperatures have a typical limit of $\sim 10^{11}$ K, mainly because of the limit of the baseline length. The space VLBI technique can measure brightness temperatures greater than 10^{12} K, and some VSOP observations show such a $T_{\rm b}$ in the compact core of blazars (Bower, Backer 1998; Shen et al. 1999).

The upper limit of the observed brightness temper-

ature is caused by the inverse Compton catastrophe (Kellerman, Pauliny-Toth 1969). Using formulae (1a) and (1b) in Readhead (1994), we can calculate the inverse Compton scattering limit as $T_{\rm b,ic} = 1.6 \times 10^{11}$ K for PKS 1741−038. In order to derive this, we adopt a synchrotron peak frequency of 15 GHz, a spectral index of −0.3 and assume a high-frequency cutoff of 100 GHz. The synchrotron turnover frequency and the spectral index are determined as follows. Hjellming and Narayan (1986) observed PKS 1741−038 at the VLA with frequencies of 1.49, 4.9, 15, and 22 GHz on 1985 October and plotted the radio spectrum in the form of flux density versus frequency. This figure indicates that PKS 1741−038 has almost the same flux densities at 15 GHz and 22 GHz, and that the flux densities at lower frequencies gradually drop. Single-dish measurements at 4.8, 8.0, and 15 GHz from UMRAO show similar flux density trends. Furthermore, 22, 37, and 87 GHz single-dish measurements at Metsähovi Radio Research Station (Teräsranta et al. 1998) indicate the highest flux density to be at 22 GHz. A flux density comparison between UMRAO 15 GHz and Metsähovi 22 GHz data shows that the 15 GHz flux density is greater than the 22 GHz flux density. An optically thin spectral index of −0.3 is obtained from these higher frequency measurements. In order to reconcile with our $T_{\rm b}$, Doppler factors, $\delta_{\rm ic}$, of 8.4 ± 1.7 (1.6 GHz), 11.7 ± 3.3 (5 GHz epoch 1), and 14.2 ± 3.4 (5 GHz epoch 2) are required. Here, we have multiplied a factor of 0.67 to convert the derived brightness temperatures, assuming a Gaussian component to an optically thin uniform sphere. If we assume that the particles and magnetic field are in equipartition we can estimate the equipartition brightness temperature limit, $T_{\rm b,eq}$ (Readhead 1994); in the case of PKS 1741−038, $T_{\rm b,eq} = 1.3 \times 10^{11}\ h^{-2/17} \delta_{\rm eq}^{0.8}$ K. From our VSOP results we can derive $\delta_{\rm eq}$ as $(18.5 \pm 4.6)\ h^{0.15}$ (1.6 GHz), $(28.1 \pm 9.7)\ h^{0.15}$ (5 GHz epoch 1), and $(35.9 \pm 10.4)\ h^{0.15}$ (5 GHz epoch 2), which are 2.5-times larger than the $\delta_{\rm ic}$ results. A third alternative is the inhomogeneous jet model (Blandford, Königl 1979); we can roughly estimate the brightness temperature limit as being $T_{\rm b,j} \sim 3 \times 10^{11} \delta_{\rm j}^{5/6}$ K, although their formula depends weakly on other observable parameters. From our VSOP results we can derive $\delta_{\rm j}$ as 6.0 ± 1.5 (1.6 GHz), 9.0 ± 3.2 (5 GHz epoch 1), and 11.4 ± 3.3 (5 GHz epoch 2), which are similar to $\delta_{\rm ic}$.

4.3. Viewing Angle

Our 5 GHz images at an interval of nine months show that there is almost no change of the structure. Previous VLBI images of PKS 1741−038 also show point-like structures. From the high Doppler factor and no structure variation, the outflow from the core of PKS 1741−038 could be directed close to our line of sight. If we assume that the apparent component motion is less than our angular resolution, we can derive the upper limit of the viewing angle, $\phi_{\rm max}$. The maximum apparent jet speed, $\beta_{\rm app,max} = 8.2$ (choosing $h = 1$ here), was derived from the minimum fringe spacing in our observations, 0.45 mas, which corresponds to 1.9 pc in the source linear scale; the observation interval between the two epochs is 275 days. Combining $\beta_{\rm app,max}$ with $\delta = 11.4$ ($\delta_{\rm j}$), 14.2 ($\delta_{\rm ic}$), and 35.9 ($\delta_{\rm eq}$), we estimate $\phi_{\rm max} = 4.^\circ 8$ (from $\delta_{\rm j}$), $3.^\circ 5$ (from $\delta_{\rm ic}$), and $0.^\circ 7$ (from $\delta_{\rm eq}$). If these are correct, it is likely that the gamma-ray emission from PKS 1741−038 is directed toward the observer, and that the emission is highly Doppler-boosted. On the other hand, we can also estimate the bulk Lorentz factors, γ, as 8.7, 9.5, and 18.9. Some theoretical considerations predict that γ is limited to less than 10 for a jet advancing into a blackbody radiation field, due to Compton drag (Phinney 1987; Melia, Königl 1989). Although we cannot conclude that PKS 1741−038 is in favor of a particular model, because the upper limit of γ is variable depending on some physical conditions, it is likely that the core region of PKS 1741−038 is not in equipartition, which gives a value about twice as large as that of the upper limit of γ.

Jiang et al. (1998) have applied the inhomogeneous jet model to 52 AGNs (including 18 EGRET AGNs), for which measurements of the angular size and radio flux density of the VLBI core, proper motion of the components in the jet, and X-ray flux density are available. They conclude that the values of δ and the bulk Lorentz factor γ of the EGRET sources are higher than those of the non-EGRET sources. The derived mean viewing angle for 14 EGRET sources is $4.^\circ 9$ and the Doppler factors of these sources is greater than 4.7. Although our VSOP result seems to be consistent with theirs, the proper motion of the outflow from PKS 1741−038 has not been reported, and our result is an upper limit of the viewing angle. It is important to continue multi-epoch observations in order to obtain conclusive results.

5. Conclusion

We performed two-epoch VSOP observations of the gamma-ray loud quasar PKS 1741−038 at an interval of nine months. The source shows almost no change of the structure, and has a brightness temperature greater than 10^{12} K at each observation. We estimated the Doppler factors by using three individual physical conditions, which provided brightness temperature limits. Doppler factors of 14.2, 35.9, and 11.4 were derived by assuming the $T_{\rm b}$ limits due to the inverse Compton catastrophe, the equipartition, and the inhomogeneous jet model, respectively. The estimated upper limit of the viewing angle of the outflow is $4.^\circ 8$, which is consistent

with the previous result of EGRET-AGNs by adopting an inhomogeneous jet model.

We gratefully acknowledge the VSOP Project, which is led by the Japanese Institute of Space and Astronautical Science in cooperation with many organizations and radio telescopes around the world. A part of this research was carried out using an observation of the VSOP Survey Program. The authors wish to thank Drs. Zhi-Qiang Shen, Shinji Horiuchi, and George A. Moellenbrock for helpful suggestions. We also thank Dr. Philip G. Edwards for useful discussions and polishing up the manuscript. The VLBA is the facility operated by Associated Universities Inc. under agreement with the National Science Foundation. This research has made use of data from the University of Michigan Radio Astronomy Observatory, which is supported by funds from the University of Michigan.

References

Blandford R.D., Königl A. 1979, ApJ 232, 34
Bower G.C., Backer D.C. 1998, ApJ 507, L117
Clegg A.W., Fey A.L., Fiedler R.L. 1996, ApJ 457, L23
Fey A.L., Clegg A.W., Fomalont E.B. 1996, ApJS 105, 299
Hartman R.C., Bertsch D.L., Bloom S.D., Chen A.W., Deines-Jones P., Esposito J.A., Fichtel C.E., Friedlander D.P. et al. 1999, ApJS 123, 79
Hirabayashi H., Hirosawa H., Kobayashi H., Murata Y., Edwards P.G., Fomalont E.B., Fujisawa K., Ichikawa T. et al. 1998, Science 281, 1825
Hjellming R.M., Narayan R. 1986, ApJ 310, 768
Impey C.D., Tapia S. 1990, ApJ 354, 124
Jiang D.R., Cao X., Hong X. 1998, ApJ 494, 139
Kellerman K.I., Pauliny-Toth I.I.K. 1969, ApJ 155, L71
Königl A. 1981, ApJ 243, 700
Linfield R.P., Levy G.S., Ulvestad J.S., Edwards C.D., DiNardo S.J., Stavert L.R.,Ottenhoff C.H., Whitney A.R. et al. 1989, ApJ 336, 1105
Melia F., Königl A. 1989, ApJ 340, 162
Moellenbrock G.A., Fujisawa K., Preston R.A., Gurvits L.I., Dewey R.J., Hirabayashi H., Inoue M., Kameno S. et al. 1996, AJ 111, 2174
Phinney E.S. 1987, in Superluminal Radio Sources, ed J.A. Zensus, T.J. Pearson (Cambridge University Press, Cambridge) p301
Readhead A.C.S. 1994, ApJ 426, 51
Shen Z.-Q., Edwards P.G., Lovell J.E.J., Fujisawa K., Kameno S., Inoue M. 1999, PASJ 51, 513
Shen Z.-Q., Wan T.-S., Moran J.M., Jauncey D.L., Reynolds J.E., Tzioumis A.K., Gough R.G., Ferris R.H. et al. 1997, AJ 114, 1999
Shepherd M.C., Pearson T.J., Taylor G.B. 1994, BAAS 26, 987
Sikora M., Begelman M.C., Rees M.J. 1994, ApJ 421, 153
Teräsranta H., Tornikoski M., Mujunen A., Karlamaa K., Valtonen T., Henelius N., Urpo S., Lainela M. et al. 1998, A&AS 132, 305
von Montigny C., Bertsch D.L., Chiang J., Dingus B.L., Esposito J.A., Fichtel C.E., Fierro J.M., Hartman R.C. et al. 1995, A&A 299, 680
White G.L., Jauncey D.L., Savage A., Wright A.E., Batty M.J., Peterson B.A., Gulkis S. 1988, ApJ 327, 561